Low-frequency superelasticity and nonlinear elastic behavior of $SrTiO_3$ crystals

A. V. Kityk
Institute of Physical Optics, Dragomanova Str 23, 290005, Lviv, Ukraine

W. Schranz, P. Sondergeld, and D. Havlik
Institut für Experimentalphysik, Universität Wien, Strudlhofgasse 4, A-1090 Wien, Austria

E. K. H. Salje
Department of Earth Sciences, University of Cambridge, Downing Street, Cambridge CB2 3EQ, United Kingdom

J. F. Scott
School of Physics, University of New South Wales, Sydney NSW 2052, Australia
(Received 6 July 1999)

To clarify the inconsistencies in existing elastic constant data of $SrTiO_3$ in the vicinity of the 105 K phase transition we have studied the temperature dependence of the Young's modulus of $SrTiO_3$ crystals. Dynamic mechanical analysis at 10–140 K and 10–45 Hz has been used for the experiments. We found two remarkable features: a giant elastic softening (superelasticity) below the cubic → tetragonal phase transition, and elastic anomalies in the quantum paraelectric region between about 25 K and 45 K. The giant elastic softening is caused by domain-wall motion: it can be suppressed with uniaxial compression and does not occur in the [111] direction. Elastic anomalies observed in the quantum paraelectric region display nonlinear elastic behavior. We relate these nonlinear elastic anomalies with the appearance of polarization clusters. Our data can be consistently described assuming a freezing of the dynamical polar clusters below 25 K.

I. INTRODUCTION

In the 1960s and 1970s the cubic → tetragonal phase transition of $SrTiO_3$ at 105 K was extensively studied and regarded as a model system for other transitions. It was assumed that this transition could be described by critical exponents obtained with renormalization group theory, following from an $n=3$, $d=3$ Hamiltonian, e.g., the theoretical value for the order-parameter exponent $\beta=0.365$.[1] Indeed Müller and Berlinger[2] using the electron paramagnetic resonance technique found an order-parameter exponent $\beta=0.33\pm0.02$.

Recently it was shown that this transition can be well described by classical Landau theory with terms up to the sixth order of the free-energy expansion, the effect of quantum saturation being included. For this purpose Salje *et al.*[3] analyzed the temperature dependence of the rotation angles of the (TiO_6) octahedra (ESR measurements), the excess diffraction intensities (synchrotron experiments), the twin obliquity (x-ray rocking curves) and the excess entropy (adiabatic calorimetry). They obtained the parameters of the free-energy expansion and found out that this phase transition of $SrTiO_3$ must be continuous and almost tricritical.

Considerable interest to these crystals has recently been resurrected in connection with the idea of a new quantum coherent state suggested by Müller *et al.*[4] Such a coherent state (often called Müller state) was expected to occur in $SrTiO_3$ below a certain temperature ($T_q\approx37$ K). At this temperature the quantum fluctuations become strong enough to prevent further critical decreasing of the soft mode frequency. As a result, the proper ferroelectric phase transition, which would be expected to occur at $T_f\approx35$ K, does not appear until $T=0$ K and the system remains in a so-called quantum paraelectric (QPE) state. The dielectric susceptibility along [110] direction saturates below T_q at extremely high values ($\chi>10^4$).

The basic idea of a quantum coherent state has been adopted from the Landau theory of superfluid helium. In particular, an analogy between the superfluid phase of ^{4}He and the quantum paraelectric state of $SrTiO_3$ was drawn. It was based on a similarity between the roton dispersion in He II and the flattening of a transverse-acoustic branch due to repulsion with the soft optical branch near the Brillouin-zone center in $SrTiO_3$, which recently has been found in a neutron-scattering experiment.[5]

Although it seems that one important criterion for the realization of a quantum coherent state is fulfilled, it is not clear whether such a state actually exists. A critical analysis of this problem has been given recently.[5] There it was proposed to relate the T_q anomalies with the existence of large polarization clusters, which render the system enormously anharmonic. Brillouin-scattering measurements revealed anomalies in the elastic constants C_{33} and C_{44} around 40 and 25 K, respectively.[6] They were attributed to the presence of polarization clusters, which lead to an interaction between the strain tensor U_{ij} and the gradient of the polarization vector P_l of the type $h_{ijkl}U_{ij}\nabla_k P_l$.[7] Recently Nes *et al.*[8] have observed distinct anomalies in the internal friction and elastic compliance of $SrTiO_3$ below 44 K, which cannot be explained by the interaction with the ordinary phonon system, including the soft mode, and the origin of these anomalies remains unclear. This explains partially our interest to test the elastic behavior of $SrTiO_3$ in the ultra-low-frequency region.

Another point concerns the different behavior of the elastic constants in the tetragonal phase of $SrTiO_3$ reported by various authors. The temperature dependences of the elastic constants of $SrTiO_3$ were studied with ultrasonic (Rehwald[9]

Scott and Ledbetter[10] Fossum *et al.*,[11] Balashova *et al.*[12]) resonant (Sorge *et al.*[13]), vibrating-reed resonant (Nes *et al.*[8]) and Brillouin-scattering (Hehlen *et al.*[6]) methods. All together these data yield information about the elastic properties in the kHz–GHz region. The controversial elastic behavior observed preferably in the kHz–MHz region is usually attributed to the uncontrolled domain structure of the sample used in the experiment. In this paper we consider some of these results in terms of the free-energy expansion of Salje *et al.*[3] and present the ultra-low-frequency (Hz region) elastic behavior of $SrTiO_3$ in a wide temperature range including the phase transition from cubic to tetragonal phase at $T_c = 105$ K. Our experimental results give clear evidence for a dominant contribution of domain-wall motion into the ultra-low-frequency elastic properties, which produces a giant softening. Special attention is paid to the analysis of the nonlinear elastic anomalies measured in the quantum paraelectric regime.

The experimental part of this work is based on dynamic mechanical analysis (DMA) measurements performed down to 15 K. Although DMA can be used for the determination of the elastic constants of a crystal, it is different from ultrasonic methods. First, the frequencies that are applied are extremely low (0.1–50 Hz) and, second, measurements always imply an oscillating external stress on the sample. No wonder the domain structure of the crystal highly depends on and can vary with the direction and the amount of the external stress. The elastic measurements are supported therefore by the results of optical microscope observation of the domain structure in these crystals.

II. EXPERIMENTAL

In the DMA method the samples are subjected to a given static force which is modulated by a dynamic force of chosen amplitude and frequency ($f = 0.1$–50 Hz). The amplitude Δh and the phase shift δ of the resulting elastic response of a sample are registered via inductive coupling with a resolution of 10 nm and 0.1^0, respectively. The knowledge of Δh and δ allows the determination of the real and imaginary parts of the elastic compliance, which can be used to calculate the Young's modulus. Measurements have been performed by a parallel plate stress (PPS) or three-point bending (TPB) arrangement (Fig. 1).

In the PPS mode the applied force produces a homogeneous stress profile $\sigma(k=0)$ within the sample leading to an elastic deformation Δh, resulting in a homogeneous Youngs modulus $Y(k=0)$, where k is the wave vector. Typical sample dimensions for PPS measurements were $S = 0.5$ mm^2 and $h = 5$ mm. In the TPB mode the applied force leads to an inhomogeneous stress in the sample with a Fourier component $\sigma(k \neq 0)$ and as a result the Youngs modulus or elastic compliance is determined at $k \neq 0$. The typical sample dimensions for the TPB method were $L = 5$ mm, $b = 1$ mm, and $h = 0.25$ mm. The relations between the effective spring constant K measured by DMA-7 and Young's modulus are determined as[14]

PPS method:

$$K = Y(\vec{\mu}) S/h, \tag{1}$$

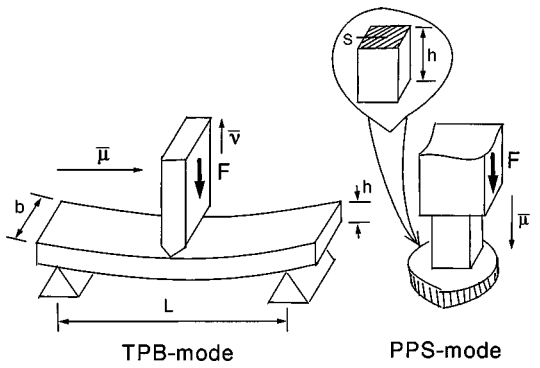

FIG. 1. Typical sample geometries for TPB and PPS methods. F is the force, b is the sample width, L is the span, d is the sample thickness, S is the base area.

TPB method:

$$K = Y(\vec{\mu}) 4b \left(\frac{h}{L}\right)^3 \left[1 + \frac{3}{2}\left(\frac{h}{L}\right)^2 \frac{Y(\vec{\mu})}{G(\vec{\mu}\vec{\nu})}\right]^{-1}, \tag{2}$$

where b, h, L, and S represent the geometrical parameters of the samples, and $G(\vec{\mu}\vec{\nu})$ is the shear modulus. Using both methods and combining different measuring geometries yields a lot of information about the elastic behavior of the measured crystal. However, since the absolute accuracy of such a measurement is usually not better than 20%, it is practically impossible to measure all components of a given elastic stiffness tensor. The relative accuracy of the DMA method is about 0.2–1% and for this reason we present all data in the relative form.

The samples were single crystals of $SrTiO_3$. They were Verneuil grown with an ultrahigh purity of 99.9998 %. The main impurities were 3 ppm of Fe and 2 ppm of Ni.

III. LANDAU FREE ENERGY AND ELASTIC ANOMALIES

The Landau expansion of the free energy F of a crystal with interacting order parameter Q and elastic strain U_i can be divided into three parts: the order-parameter part F_Q, the elastic energy F_U, and the interaction energy F_{QU} between the order parameter and the strain.

The phase transition of $SrTiO_3$ at 105 K is accompanied by a symmetry reduction $Pm\bar{3}m \rightarrow I4/mcm$. The transition is improperly ferroelastic. It is associated with the instability of the soft mode at the R point $(\frac{1}{2},\frac{1}{2},\frac{1}{2})$ of the Brillouin zone. The active representation for such a nonequitranslational phase transition is the three-dimensional representation T_{1g} of the space group $Pm\bar{3}m$. The relevant part of the free-energy expansion F can be written as[15]

$$F = F_Q + F_U + F_{QU}, \tag{3}$$

$$F_Q = \frac{1}{2}a(T - T_c)(q_1^2 + q_2^2 + q_3^2) + \frac{1}{4}b_1(q_1^2 + q_2^2 + q_3^2)^2$$

$$+ \frac{1}{4}b_2(q_1^4 + q_2^4 + q_3^4) + \frac{1}{6}c(q_1^6 + q_2^6 + q_3^6),$$

TABLE I. Free energy coefficients.

$C_{11}^0=C_{22}^0=C_{33}^0=3.18\times10^{11}$ N m^{-2}	$B=1.229\times10^6$ J m^{-3}
$C_{12}^0=C_{13}^0=C_{23}^0=1.02\times10^{11}$ N m^{-2}	$a_1=a_2=9.973\times10^7$ J m^{-3}
$A_0=1.95\times10^4$ J K^{-1} m^{-3}	$a_3=-1.413\times10^8$ J m^{-3}
$B'=8.69\times10^5$ J m^{-3}	
$C=1.17\times10^6$ J m^{-3}	
$T_c=105.6$ K	
$\theta_s=60.75$ K	

$$F_U=\frac{1}{2}(C_{11}^0-C_{12}^0)(U_0^2+U_t^2)+\frac{1}{2}C_a^0U_a^2+\frac{1}{2}C_{44}^0(U_4^2+U_5^2+U_6^2),$$

$$F_{QU}=\lambda_1U_a(q_1^2+q_2^2+q_3^2)+\lambda_2[\sqrt{3}U_0(q_1^2-q_2^2)+U_t(2q_3^2-q_1^2-q_2^2)]+\lambda_3(U_6q_1q_2+U_5q_1q_3+U_4q_2q_3),$$

where $U_0=(U_1-U_2)/\sqrt{2}$, $U_t=(2U_3-U_1-U_2)/\sqrt{6}$, $U_a=(U_1+U_2+U_3)/\sqrt{3}$, and $C_a^0=C_{11}^0+2C_{12}^0$. For the sake of simplicity only one sixth-order term is considered in the expansion of the Landau potential F_Q. F_U can be reduced to the simple and often used expression, i.e., $(1/2)C_{ij}^0U_iU_j$ (where C_{ij}^0 is the elastic constant tensor in cubic symmetry).

The symmetry change $Pm\bar{3}m\rightarrow I4/mcm$ requires $q_1=q_2=0$ and $q_3^2=(a/b^*)(T_c-T)$ with $b^*=b_1+b_2-[8\lambda_2^2/(C_{11}^0-C_{12}^0)]$. We can, therefore, reduce the three-component order parameter to a scalar ($Q=q_3$).

With these simplifications and taking quantum saturation into account[3] we get the following expression for the free energy:

$$F=\frac{1}{2}A_0\theta_s\left(\coth\frac{\theta_s}{T}-\coth\frac{\theta_s}{T_c}\right)Q^2+\frac{1}{4}BQ^4+\frac{1}{6}CQ^6+a_1(U_1+U_2)Q^2+a_2U_3Q^2+\frac{1}{2}\sum_{i,j=1}^{3}C_{ij}^0U_iU_j, \quad (4)$$

where θ_s is the Debye temperature and $B=b_1+b_2$. The new coupling constants a_1 and a_2 are expressed in terms of the initial constants λ_1 and λ_2 as $a_1=\lambda_3/\sqrt{3}-2\lambda_2/\sqrt{6}$ and $a_2=\lambda_3/\sqrt{3}+4\lambda_2/\sqrt{6}$. The first term in Eq. (4) considers the quantum saturation in the displacive limit.[3] Quantum saturation becomes very important in the low-temperature region. Coupling terms with nondiagonal strain components (U_4, U_5, and U_6) in the expansion (3) represent the contributions to the shear elastic constants C_{44}, C_{55}, and C_{66}. Since we do not analyze the behavior of shear elastic constants the corresponding coupling terms are omitted.

The behavior of the elastic constants C_{ij} can be derived using the Slonczewski-Thomas equation[16]

$$C_{ij}=C_{ij}^0-\frac{1}{1+i\omega\tau_Q}\frac{\partial^2F}{\partial U_i\partial Q}\left(\frac{\partial^2F}{\partial Q^2}\right)^{-1}\frac{\partial^2F}{\partial Q\partial U_j}, \quad (5)$$

which in the static limit ($\omega\tau_Q\ll1$) yields

$$C_{ij}=C_{ij}^0-\frac{2a_ia_j}{(B+2C\langle Q^2\rangle)}, \quad (6)$$

where

$$\langle Q^2\rangle=\frac{-B'+\sqrt{B'^2-4CA_0\theta_s[\coth(\theta_s/T)-\coth(\theta_s/T_c)]}}{2C} \quad (7)$$

is the equilibrium value of the order parameter. Many of the coefficients appearing in the free-energy expansion (4) were determined by Rehwald[9] and Salje *et al.*[3] (cf. Table I, left column).

We have determined all other necessary coefficients from the results of dilatometric measurements[17] and the data presented in the left column of Table I, using the following relations:

$$U_i^0=S_{ij}^0a_j\langle Q^2\rangle,$$

$$B=B'+2a_iS_{ij}^0a_j, \quad (8)$$

where S_{ij}^0 is the compliance in the cubic system. After evaluation of all relevant parameters of the free energy we calculate the elastic constants and compliances as functions of temperature. Figures 2 and 3 present the results of these calculations in comparison with published experimental data (Rehwald[9]; Nes *et al.*[8]; Scott and Ledbetter[10]).

Equation (6) predicts a negative jump for C_{12} and a positive one for C_{13}. It contains only positive parameters except a_i and a_j. Since $a_1=a_2>0$ and $a_3<0$ (cf. Table I), we can conclude that the second term will be positive, provided that $i=1,2$ and $j=3$ or vice versa, i.e., for $C_{13}=C_{23}=C_{31}=C_{32}$. C_{12}, by comparison, will show a negative jump at the phase transition.

The elastic constants and compliances almost quantitatively agree with the experimental data obtained by Rehwald,[9] provided that we interchange the two crystallographic base vectors **b** and **c** with each other. This implies the interchange of the elastic constants $C_{11}\rightarrow C_{33}$ and $C_{12}\rightarrow C_{13}$.

Similar considerations apply to the other experimental data: If we interchange the base vectors **b** and **c** with each other, we get a better accordance of the measured elastic compliances with the calculated ones (Fig. 2), at least at temperatures very far below T_c. At temperatures just below T_c the experimental data differ considerably from one another. Rehwald[9] and Nes *et al.*[8] present a similar jump of the elastic compliance S_{11} at T_c, i.e., $\Delta S_{11}\approx0.25\,S_{11}^0$, which is close to the jump of S_{33} calculated by us. Scott's S_{11} by

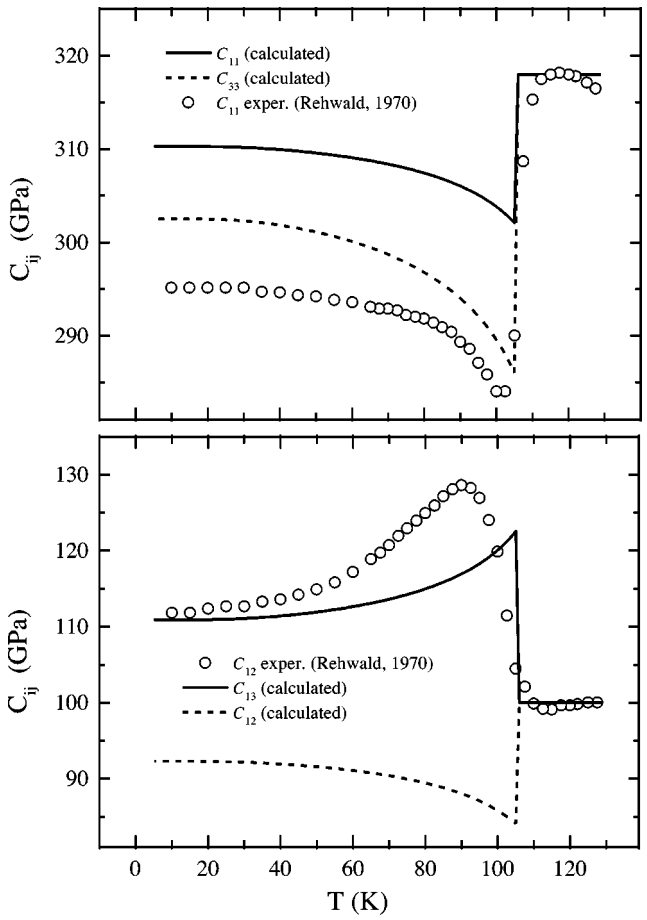

FIG. 2. Elastic constants of $SrTiO_3$ crystals measured by Rehwald (Ref. 10) and calculated using the free-energy coefficients presented in Table I.

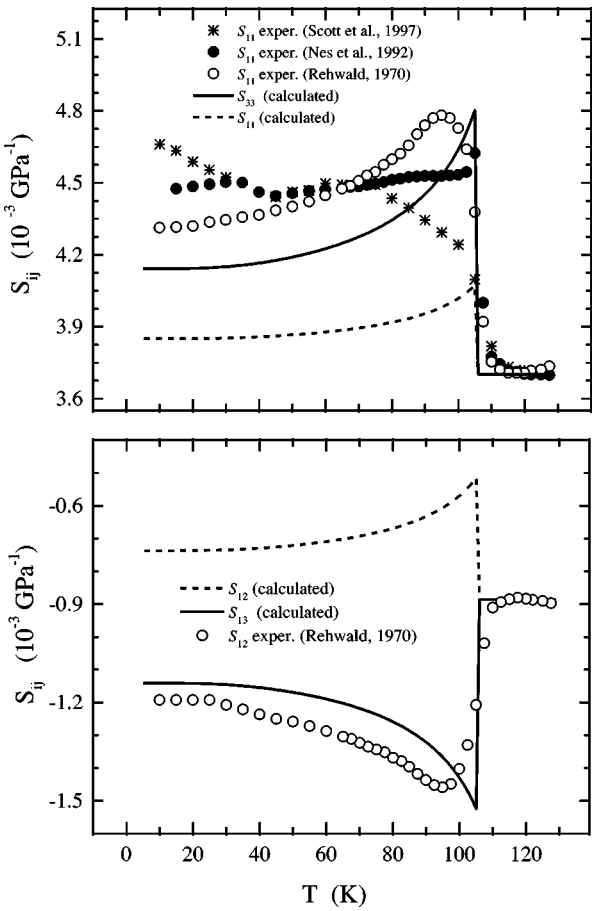

FIG. 3. Elastic compliances of $SrTiO_3$ crystals measured by Rehwald (Ref. 10), Nes *et al.* (Ref. 9), Scott and Ledbetter (Ref. 11) and calculated using the free-energy coefficients presented in Table I.

contrast appears to change continuously from S_{11} (calc.) at T_c to S_{33} (calc.) at very low temperatures. The above-mentioned experimental data have been obtained by ultrasonic and vibrating-reed resonant methods, i.e., with frequencies in the MHz and kHz region, respectively. Since the measuring conditions are comparable with each other the reason for the differences of the data most likely must be found in the different properties of the crystals. None of the above-mentioned authors has checked the domain structure and the domain-wall motions of the crystal that can have considerable influence on the elastic behavior. Particularly, as we show below, the domain-wall movement can produce a giant contribution to the elastic anomalies in the ultralow frequency limit. Rehwald,[9] whose experimental data agree pretty well with our calculations, assumes a ''pseudocubic'' crystal, i.e., a crystal with equal volume portions of the domain types. In our opinion a more or less single-domain crystal, with a confusion of two crystallographic axes (**b** and **c**), would be more plausible.

IV. TWIN STRUCTURE IN THE TETRAGONAL PHASE

In the low-temperature tetragonal phase of $SrTiO_3$ there are three types of orientational domains with two different translations each. The domain structure thus contains ferroelastic domains and antiphase domains. Our further attention will be devoted to the ferroelastic domain walls, since only their movement is possible under external stress, creating thus significant contribution to the elastic anomalies.

We have performed temperature-dependent optical microscope observations of $SrTiO_3$ crystal plates.[18] The domain structure in $SrTiO_3$ in the bulk of the sample consists of coarse ferroelastic domains. We found almost no memory of the domain patterns under repeated heating and cooling through the transition point. The most common structure were arrays of parallel domain walls leading to the formation of needle domains near to the crystal surface. The domain walls showed no temperature dependence between 8 K$<T<$103.4 K (see Fig. 4). At the temperature between 103.4 K and T_c the contrast between the birefringence of two adjacent domains is too weak to allow the visual observation of the domain walls.

V. DYNAMIC MECHANICAL ANALYSIS

The temperature dependences of the relative Young's modulus $Y^r_{[100]} \equiv Y_{[100]}(T)/Y_{[100]}$ (130 K) obtained by the TPB and PPS methods are presented in Fig. 5. In this case the changes of the Young's modulus $Y^r_{[100]}(T)$ are associated with the temperature behavior of the relative elastic compliance $S^r_{11}(Y_{[100]} \equiv 1/S^r_{11})$.

Both methods show practically the same qualitative behavior of $Y^r_{[100]}(T)$ in the low-temperature phase, although

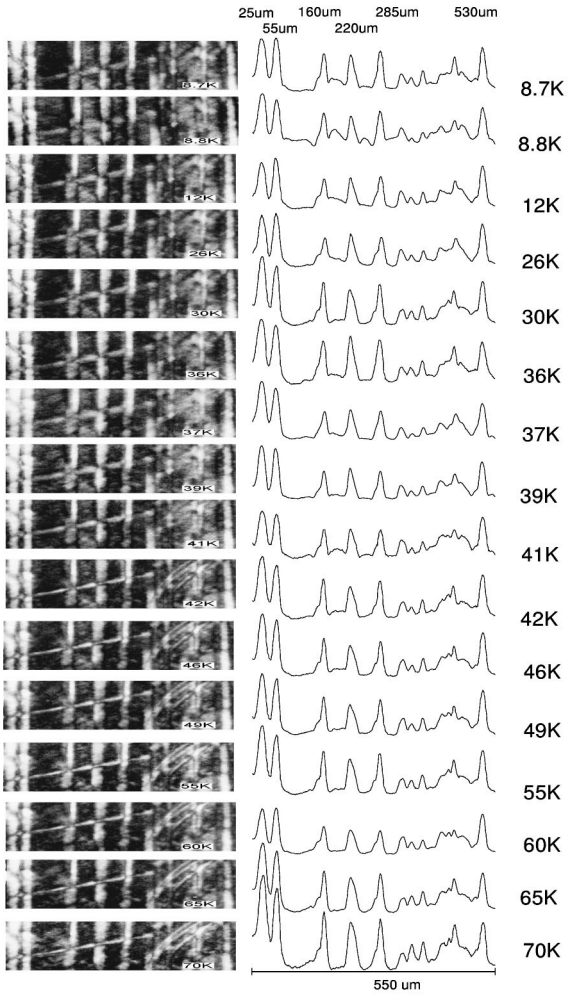

FIG. 4. The photomicrographs on the left show a twinned area of $SrTiO_3$ at different temperature increments. Each image is 550 μm wide. Some surface scratching is also visible. The intensity profiles extracted from these images are displayed on the right side. From Ref. 18.

some quantitative difference is observed. Nevertheless, the relative changes of Young's modulus obtained by both these methods exceed the anomalies expected from the phenomenological theory and those obtained in high-frequency measurements[8–10] by almost an order of magnitude. Moreover, the same qualitative and quantative changes take place also for the Young's modulus along the directions [110] and [112] measured by the TPB method. The temperature dependences of the relative Young's modulus $Y^{r}_{[112]}(T)$ are presented in Fig. 6 for two fixed frequencies of 10 and 45 Hz.

It is immediately obvious that the elastic behavior along this direction has nearly the same character as for the [100] direction and is practically frequency independent in the range 5–50 Hz. It should be stressed that weak anomalies in the real part and more pronounced anomalies in the imaginary part of the Young's modulus $Y^{r}_{[100]}(T)$ appear also in the TPB geometry in the low-temperature region (between about 25 and 45 K). They will be considered in more detail in the next section. The giant anomalous softening, which appears immediately below T_c, can easily be suppressed by external static stress (dc component of stress) applied in the same geometry as the measuring ac component of stress (Fig. 7).

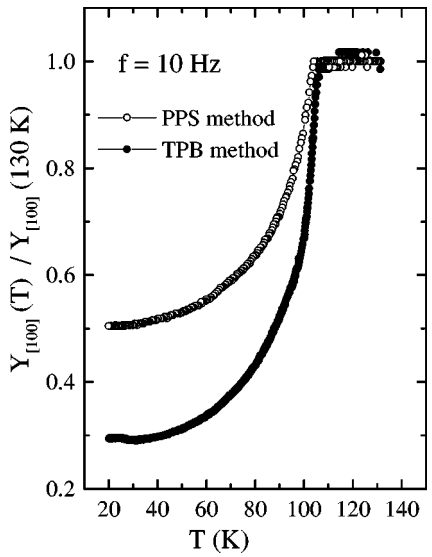

FIG. 5. Temperature dependence of the relative Young's modulus $Y^{r}_{[100]}$ of $SrTiO_3$ crystals measured by PPS and TPB method at $f = 10$ Hz.

In the case of very high values of static stress $Y^{r}_{[112]}(T)$ displays nearly monodomain behavior. The magnitude of the jump at T_c of 6–8% is close to the one which has been obtained from our numerical estimations and is also close to the high-frequency elastic constants data.[8–10] The particular influence of external stress on the elastic behavior below T_c confirms the idea of domain-wall contributions to the total elasticity. An important observation was that by releasing the static stress at any temperature in the tetragonal phase the initial value (for multidomain structure) of the Young's

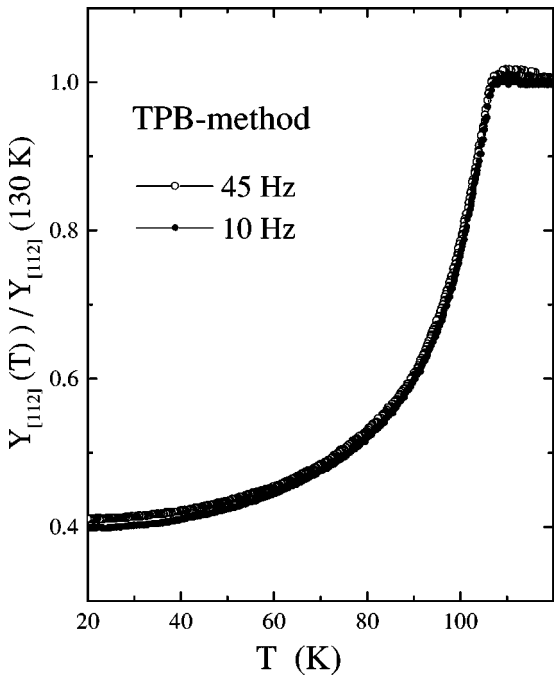

FIG. 6. Temperature dependence of the relative Young's modulus $Y^{r}_{[112]}$ of $SrTiO_3$ crystals measured by the TPB method at $f = 10$ and 45 Hz.

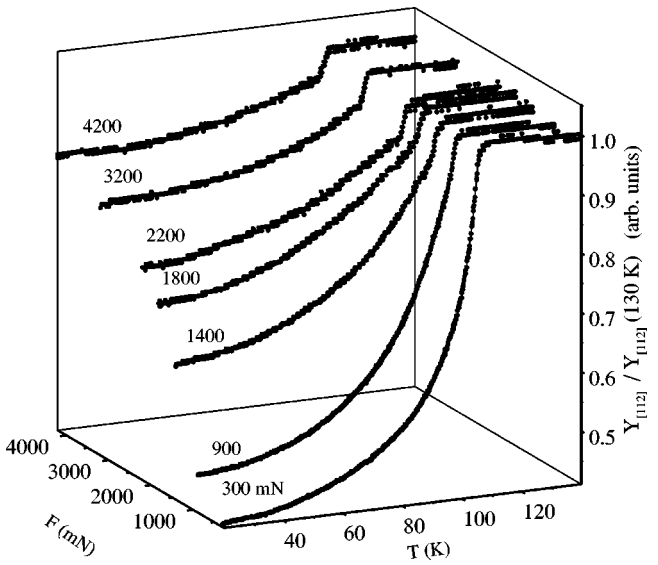

FIG. 7. Temperature dependence of the relative Young's modulus $Y^r_{[112]}$ of $SrTiO_3$ crystals measured with different static loads $F_s(\sigma_s \propto F_s)$ by the TPB method ($f=11$ Hz, crystal size: $6.7\times1.5\times0.44$ mm^3).

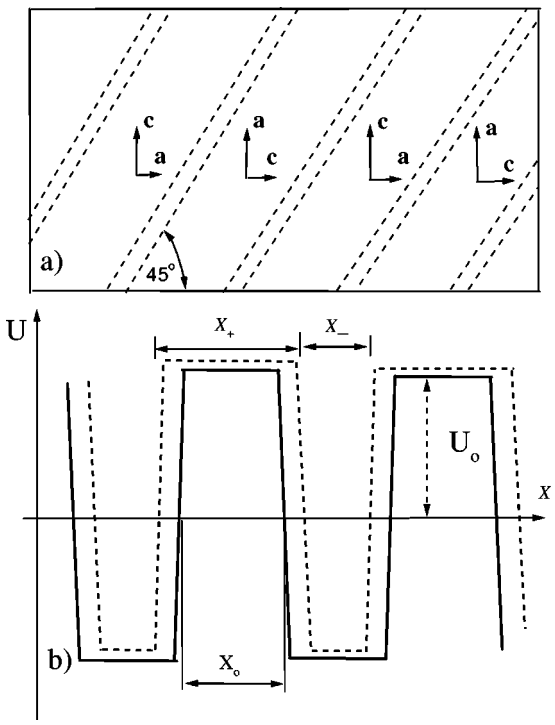

FIG. 8. (a) Schematic representation of the sequence of ferroelastic domain walls in the low-temperature tetragonal phase of $SrTiO_3$, (b) distortion of the domain structure under external stress.

modulus was recovered. The domain formation in $SrTiO_3$ is rather stable with respect to the applied stress. In this sense the domain structure behaves quite similarly to a soliton structure of improper incommensurate ferroelastics.[19] Due to the anomalous giant elastic softening in the tetragonal phase of $SrTiO_3$ this state can be characterized as a superelastic one. To calculate the domain-wall contribution to the elastic behavior let us consider a simplified configuration of the domain structure containing a sequence of only two types of domains: with ac and ca orientation, respectively [Fig. 8(a)]. Such a sequence indeed forms the twin structure in $SrTiO_3$. The profile of periodic longitudinal strains along a chosen X direction ($U\equiv U_{xx}$) is shown in Fig. 8(b).

The amplitude of the modulation is $U_0=(U_c-U_a)/2$. Under an applied stress $\sigma=\sigma_s+\delta\sigma$ (σ_s and $\delta\sigma$ are the static and oscillating parts, respectively), the width x_+ of domains with $U(+)$ enlarges, whereas the width x_- with $U(-)$ shrinks [Fig. 8(b)]; $x_++x_-=2x_o$ corresponds to the new periodicity of the domain structure. We assume that x_0 is a function of the static stress σ_s only and does not depend on the oscillating part of the stress $\delta\sigma$ [i.e., $(\partial x_+/\partial\sigma)_{x_0}=-(\partial x_-/\partial\sigma)_{x_0}$], which is obviously valid for small amplitudes of dynamical stress. The macroscopic strain of the system due to the domain wall shift is

$$\Delta U=\frac{U_0(x_+-x_-)}{x_++x_-}=\frac{U_0}{x_0}\Delta x, \tag{9}$$

where Δx is the domain-wall shift under dynamical stress. Thus the contribution to the compliance due to the domain-wall movement can be determined as

$$\Delta S_D=\frac{U_0}{x_0}\frac{\Delta x}{\Delta\sigma}, \tag{10}$$

where according to Eq. (8) $U_0\propto\langle Q^2\rangle$. Here the ratio $\Delta\sigma/\Delta x$ is proportional to the effective spring constant k_D of interkink interaction and x_0 is the interkink distance. In the previous section we concluded already that the interwalls distance x_0 remains nearly constant in the whole range of the tetragonal phase. We have fitted our experimental results according to equation $Y^r_{[100]}=(1+\Delta S^r_{LK}+\Delta S^r_D)^{-1}$, where ΔS^r_{LK} and ΔS^r_D are the relative contributions due to the relaxational LK mechanism and domain-wall movement mechanism, respectively (Fig. 9).

One obtains excellent agreement between the experimental and the calculated values of $Y^r_{[100]}$. The parameter $\Delta x/x_0\Delta\sigma$ turned out to be independent of temperature. This is in agreement with the observation that the domain structure remains unchanged in the whole tetragonal phase. It is important to note that no domain freezing (hardening of the Young's modulus) was detected down to 15 K.

At the end of this section we make some remarks concerning the quantitative difference in the Young's modulus measured by the PPS and TPB methods. We explain it by the different character of strain distribution inside the sample, which indeed takes place in both of these methods. Remember that in the case of the PPS method the strain is nearly homogeneous over almost all volumes of the sample, whereas for the TPB method it is strongly inhomogeneous. This results in differences in the character of the domain-wall movement, which schematically for a simple one-dimensional domain sequence is shown in Fig. 10.

One observes that in PPS geometry only parallel shifts of domain walls occur [Fig. 10(b)], whereas in the TPB mode twin boundaries tilt in opposite directions under an applied load [Fig. 10(c)]. No doubt that in both cases the effective spring constant k_D is different, which most likely is the reason for the quantitative difference in the magnitudes of the Young modulus determined by the PPS and TPB methods,

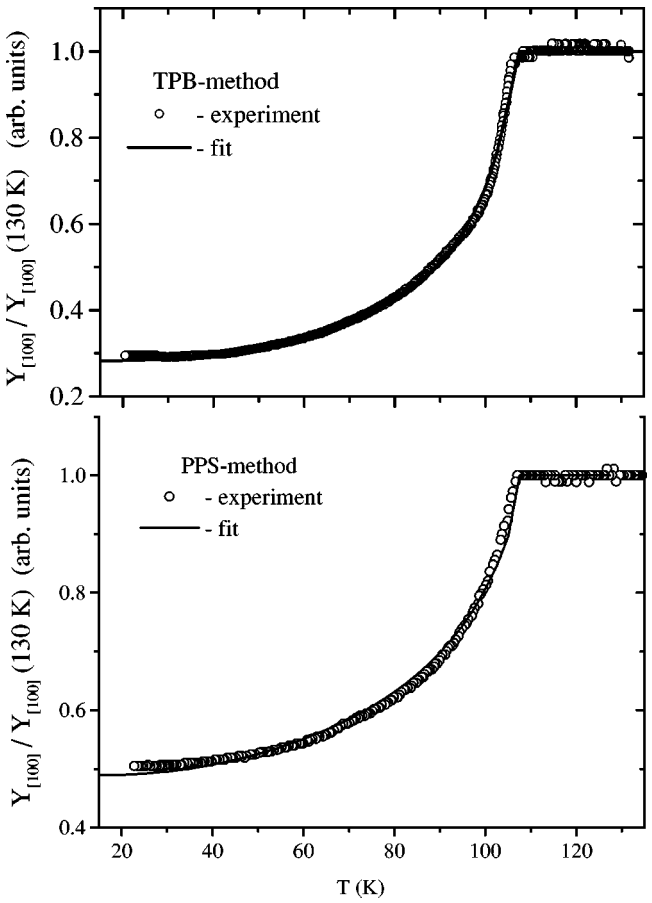

FIG. 9. Temperature dependence of the relative Young's modulus $Y^{r}_{[100]}$ (TPB and PPS methods) measured and calculated according to Eqs. (8) and (12) (see text).

respectively. In a special case such a difference is striking, particularly, if the compression occurs along the crystallographic [111] direction (Fig. 11).

One observes that the anomalous change of the Young's modulus $Y_{[111]}$ measured by the PPS method is nearly five

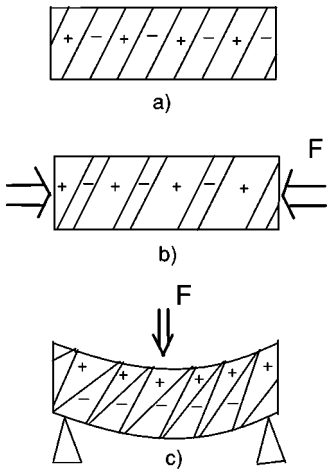

FIG. 10. (a) Schematic representation of the sequence of ferroelastic domain walls in the low-temperature tetragonal phase of $SrTiO_3$ for two different types of their distortion: (b) under homogeneous stress (PPS mode) and (c) in the presence of the bending (inhomogeneous) deformation (TPB mode).

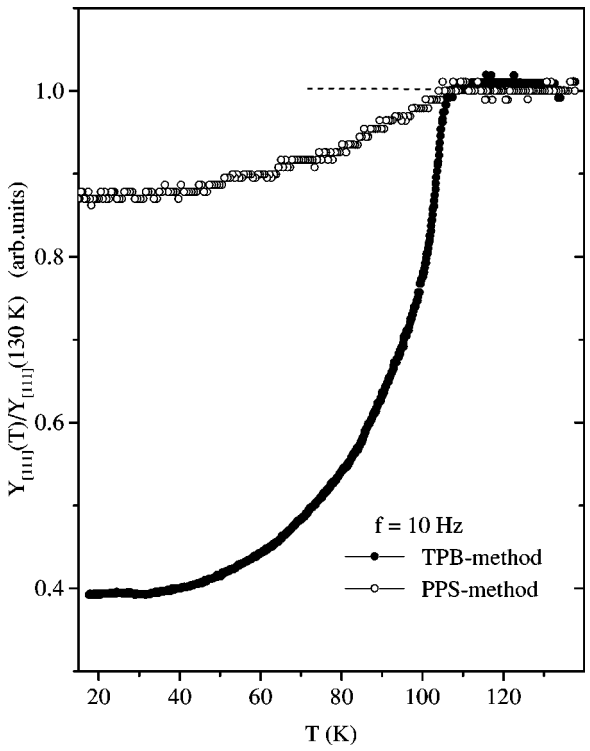

FIG. 11. Temperature dependence of the relative Young's modulus $Y^{r}_{[111]}$ of $SrTiO_3$ crystals measured by the PPS and TPB method at $f=10$ Hz.

times smaller in comparison with the one obtained in the TPB geometry. Note that a simple estimation gives in this direction the value for the LK jump of about 2%, which is below the experimental resolution for the PPS mode. This experimental fact is an excellent confirmation for the different types of domain-wall movements which must occur in both of these methods. In the PPS mode the homogeneous stress along the [111] direction is not able to move walls at all, since it does not prefer any of the existing three types of domain orientations. In this case we can say that the domain-wall contribution is suppressed ''geometrically.'' Contrary, in the TPB mode the inhomogeneous stress having both longitudinal and shear components still produces considerable domain-wall movement which results in the superelasticity of $SrTiO_3$.

VI. LOW-TEMPERATURE ELASTIC ANOMALIES

In addition to the giant softening, a smaller elastic anomaly was observed in the temperature range of about 25–45 K. Figure 12 shows the low-temperature part of the relative Young's modulus $Y^{r}_{[100]}(T)$ obtained by the PPS and TPB methods. One observes an additional weak softening only in the TPB geometry. The behavior is reproducible, and the anomalies in the real part are accompanied by the anomalies in the imaginary part $Y''_{[100]}=Y^{r}_{[100]}\tan\delta$ (Fig. 13) in the same temperature range.

A pronounced decrease in $Y''_{[100]}(T)$ between 25 and 50 K occurs here additionally to the anomalous peak observed in the region of the cubic-tetragonal phase transition at $T=T_c$. No losses have been revealed in the PPS geometry. We also have not observed anomalies along two other direc-

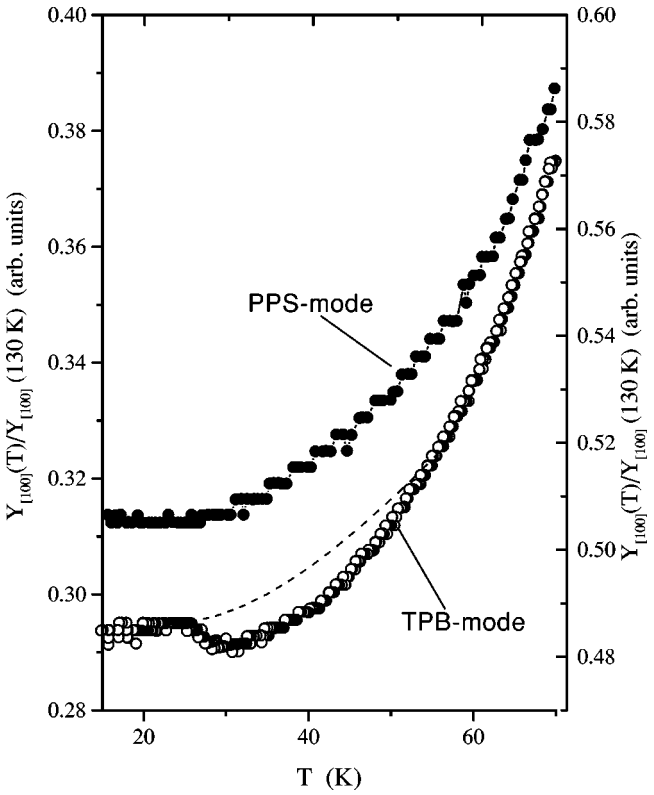

FIG. 12. Detailed plots of the temperature dependence of the relative Young's modulus $Y^{r}_{[100]}$ of $SrTiO_3$ crystals measured by the PPS and TPB methods ($f=11$ Hz) in the low-temperature region.

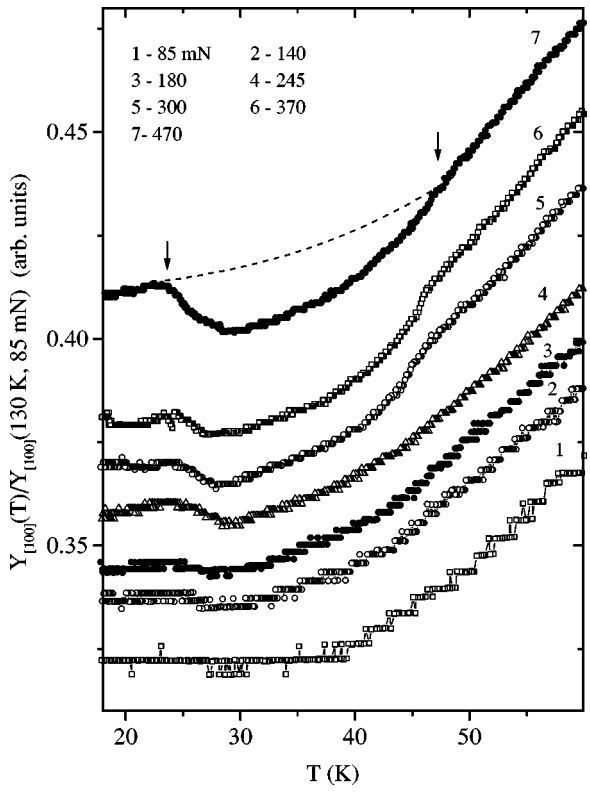

FIG. 14. Temperature dependence of the relative Young's modulus $Y^{r'}_{[100]}$ of $SrTiO_3$ crystals measured by the TPB method ($f=11$ Hz) at different amplitudes of the dynamic load δF.

tions, i.e., parallel to the [111] and [112] directions. In addition, for TPB geometry we have revealed a strong dependence of both real and imaginary parts of the elastic constants on the amplitude of dynamic stress (Figs. 14 and 15).

It turns out that at low enough amplitudes of the dynamic load (less than about 100 mN for a sample with dimensions: $L=5$ mm, $b=1$ mm, $h=0.27$ mm), the elastic anomalies do not appear even in the TPB mode. In the PPS mode the magnitudes of stresses are usually one or two orders less,

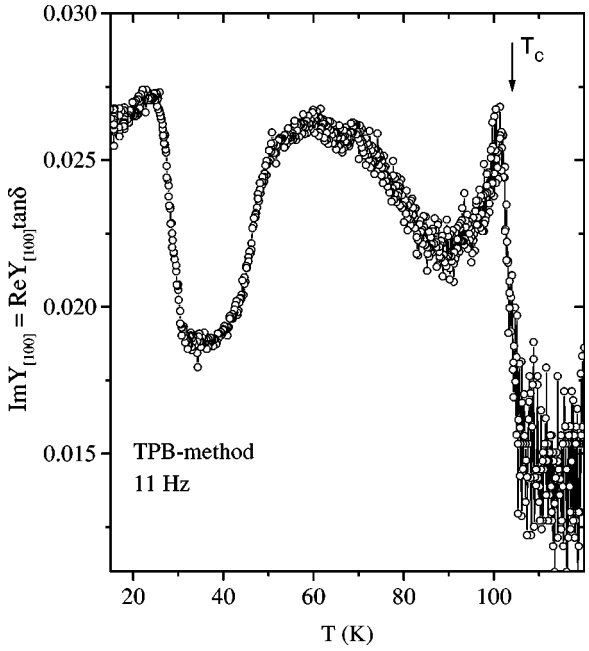

FIG. 13. Temperature dependence of the imaginary part of the complex Young's modulus $Y^{r}_{[100]}$ of $SrTiO_3$ crystals measured by the TPB method at $f=11$ Hz.

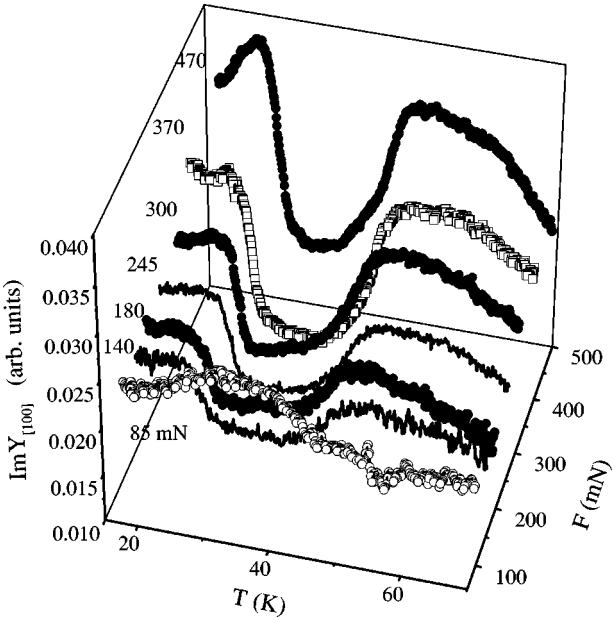

FIG. 15. Temperature dependence of the imaginary part of the Young's modulus $Y^{r'}_{[100]}$ of $SrTiO_3$ crystals measured by the TPB method ($f=11$ Hz) at different amplitudes of the dynamic load δF.

which partially explains why these anomalies are not observed in such a geometry. Another reason for this will become clear below. The data shown in Figs. 14 and 15 thus represent clear nonlinear elastic behavior.

The high-temperature anomalous peak in the imaginary part is clearly related with the cubic-tetragonal transition and most probably must be attributed to the interaction (friction) of ''mobile'' twin walls with defect and discrete lattice structure.[21]

What could be the origin of the observed nonlinear low-temperature elastic behavior of $SrTiO_3$? Immediately one can exclude the following mechanisms:

(i) The observed low-temperature anomalies are clearly not related with the adiabatic-isothermal crossover. The corresponding estimations yield extremely small magnitudes of the contributions into the elastic modulus due to the small thermal expansivity, especially in the low-temperature region.

(ii) Domain freezing cannot account for the observed anomalies. The considerable contribution of domain-wall motion to the elastic constant is still observed in the low-temperature region (see Figs. 5 and 6).

According to the results of neutron-scattering measurements[22] $SrTiO_3$ exhibits a rather strong TO-TA coupling, which partially can be described by the coupling term $\propto U_j \nabla_k P_l$, where P_l is the polarization vector, and U_j is a component of the strain tensor. One expects that approaching T_q polarization clusters become increasingly important, which indeed leads to the extremely high dielectric permittivity. Estimations have shown that at low temperatures the cluster polarization $\langle P^2 \rangle$ is large in $SrTiO_3$.[5] The neutron experiments suggest that QPE clusters render the system enormously anharmonic. Brillouin scattering shows that the coupling of strain to polarization is sufficiently nonlinear for small wave vectors, being mediated by the clusters themselves.[22] Naturally, it comes to mind that the nonlinear elastic behavior is related with the QPE clusters.

Before considering the influence of paraelectric clusters to the nonlinear elastic behavior the following fact must be stressed. In the TPB geometry the external load F creates a linear strain gradient inside the sample (Fig. 16), i.e., $U_{[100]}(z) \propto \sigma_0 (z - h/2)$.

In Fig. 16 the gradient interactions are given for three types of orientational domains. Such a strain gradient creates a perfect homogeneous polarization along the [001] direction (due to the invariants presented in Fig. 16 for the three types of domains). Therefore, the influence of the strain gradient is equivalent to the action of an external homogeneous electric field along the [001] direction. In liquid crystals this is known as the flexoelectric effect.[20] It was established that an electric field has strong influence on the ferroelectric soft-mode behavior, i.e., $\omega_{\mathrm{TO}}^2(T,E) = \omega_{\mathrm{TO}}^2(T,0) + \Delta(E,T)$ where $\Delta(E,T) \propto E^2/\omega_{\mathrm{TO}}^4(T,E)$.[23] Since $E \propto \sigma_o$, then $\Delta(E,T) \equiv \Delta(\sigma_o,T)$. Therefore, the polarization fluctuations $\langle \delta P_i^2(T) \rangle \propto k_B T/\omega_{\mathrm{TO}}^2(T,E)$ $(i=x,y)$ are strongly dependent on the applied electric field, which in our case is equivalent to the applied stress. We have calculated the stress, which appears in the sample in a three-point bending experiment using the relation $\sigma = 3FL/bd^2$.[24] With $F = F_s + \delta F(t)$ and $\delta F = 85 - 470$ mN we obtain maximal stresses between 0.07 and 0.12 GPa. Extremely high magnitudes of the strains at

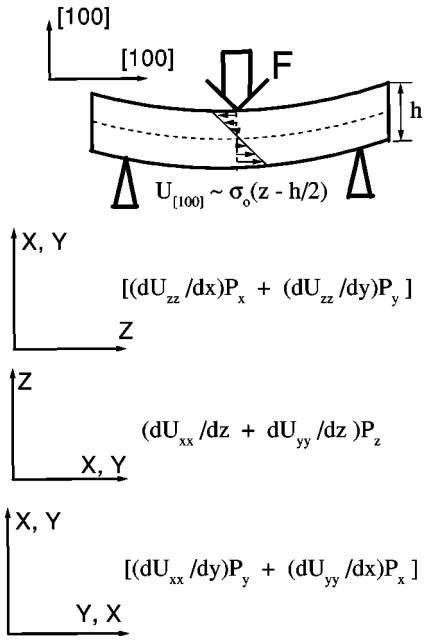

FIG. 16. Strain gradient leading to the appearance of a homogeneous polarization along [001] direction in three-point bending. The corresponding linear gradient invariants are presented for three orientational types of domains.

the sample edges together with small sample thickness lead to large values of the induced polarization. Assuming that P^2U^2 interactions dominate the elastic constant behavior of $SrTiO_3$ at low temperatures, we obtain

$$\Delta Y^* \propto \langle \delta P_i^2(T) \rangle \propto \frac{k_B T}{\omega_{\mathrm{TO}}^2 + \Delta(\sigma_0)/(1 + i\omega\tau)}. \qquad (11)$$

Equation (11) can be reduced to the more suitable Debye form by introducing the renormalized stress-dependent relaxation time $\tau^* = \tau \omega_{\mathrm{TO}}^2 / [\omega_{\mathrm{TO}}^2 + \Delta(\sigma_0)]$ leading to

$$\Delta Y^* \propto \frac{k_B T}{\omega_{\mathrm{TO}}^2} - \frac{k_B T \Delta(\sigma_0)}{\omega_{\mathrm{TO}}^2 [\omega_{\mathrm{TO}}^2 + \Delta(\sigma_o)]} \frac{1}{1 + i\omega\tau^*}. \qquad (12)$$

The first term corresponds to the linear contribution, whereas the second one is a nonlinear relaxation contribution to the elastic modulus. Equation (12) implies that we measure the polarization fluctuations in the presence of a time-dependent inhomogeneous strain. Physically, it has the following meaning: if $\omega\tau^* \ll 1$ (τ^* is the life time of the polarization clusters) the polarization clusters feel the electric field like a static field and are periodically suppressed under dynamic loading. For $\omega\tau^* \gg 1$ the dynamics of polarization clusters is slow compared to the time-dependent strain gradient, implying that they do not feel the electric field at all. Figure 17 shows the temperature dependences of the real and imaginary parts of the complex modulus calculated according to Eq. (12). One obtains a good correspondence to the experimental data (Figs. 14 and 15).

Note that even the shifts of the anomalies with increasing stress are nicely reproduced. The anomalous peak in the temperature dependence of the imaginary part at about 25 K appears at $\omega\tau^* = 1$, i.e., it can be attributed to the freezing of the polarization clusters. Other evidence for polarization

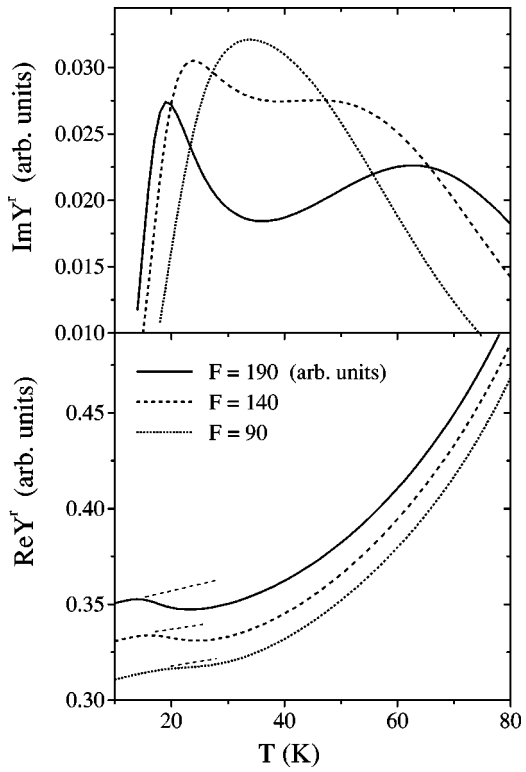

FIG. 17. Temperature dependences of the real and the imaginary parts of the complex Young's modulus calculated according to Eq. (12).

clusters in $SrTiO_3$ have been obtained recently from dielectric loss measurements near 25 and 40 K.[25]

VII. SUMMARY

Although the temperature dependence of the elastic constants of $SrTiO_3$ was measured extensively by various authors, there was no clear picture about the elastic behavior of these crystals near the 105 K phase transition. In our opinion the observed discrepancies are due to the occurrence of ferroelastic domains appearing below T_c. Using the parameters determined by Salje *et al.*[3] for the Landau expansion of $SrTiO_3$, we have calculated the temperature dependences of the elastic constants. A comparison with the experimental data shows that the high-frequency (MHz region) elastic behavior of $SrTiO_3$ can be well described by Landau theory with terms up to sixth order and the free-energy parameters of Salje *et al.*[3]

The low-frequency elastic behavior, however, turns out to be quite different and cannot be described by simple Landau theory. A giant (superelastic) softening appears in the tetragonal phase at low frequencies (Hz region). It was never observed before in these crystals at higher frequencies (i.e., in the kHz–GHz region). To explain it, we have calculated the elastic response of a crystal containing a number of ferroelastic domain walls. The resulting anomaly in the elastic compliance was obtained to be proportional to the spontaneous strain U_0 and inversely proportional to the domain-wall distance x_0 and the domain-wall interaction k_D. Fitting our data with $\Delta S_D=[U_0/(x_0k_D)\propto(x_0k_D)^{-1}\ \langle Q^2\rangle]$, we obtained excellent agreement over a large temperature range ($T=15$ K to $T=T_c$). Here the temperature dependence of the order parameter Q was calculated from the free-energy expansion of Ref. 3 and the fit parameter $1/x_0k_D$ turned out to be temperature independent in the whole tetragonal phase. This is in good agreement with the optical microscope observations of the twin structure which revealed no changes in the size of domains in the whole region of the tetragonal phase.

We have also detected elastic anomalies in the low-temperature range between 25 and 45 K at relatively high amplitudes of the applied dynamic stress. An anomalous behavior has been observed only in the three-point bending geometry in both real and imaginary parts of the complex Young's modulus. No anomalies were observed at sufficiently small amplitudes of the dynamic stress and in parallel-plate geometry. The obtained results thus represent clear nonlinear elastic behavior in the quantum paraelectric regime. In our opinion the origin of the elastic anomalies is related with polarization clusters which are increasingly large in the quantum paraelectric region. The nonlinear character of the elastic anomalies appears due to the fact that the quantum paraelectric clusters are dynamically suppressed under the action of the applied time dependent strain gradient, which due to the flexoelectric coupling is equivalent to the action of a time-dependent homogeneous electric field. Below 25 K the dynamical polar clusters appear to be frozen on the time scale of our experimental range of frequencies.

ACKNOWLEDGMENTS

The present work was carried out in the frame of the EU Network on Mineral Transformations (Contract No. ERB-FMRX-CT97-0108). Support from Österreichischer Fonds zur Förderung der Wissenschaftlichen Forschung, Project No. P12226-PHY is gratefully acknowledged.

[1] A. Aharony, in *Phase Transitions and Critical Phenomena*, Vol. 6, edited by C. Domb and M.S. Green (Academic, New York, 1976).
[2] K.A. Müller and W. Berlinger, Phys. Rev. Lett. **26**, 13 (1971).
[3] E.K.H. Salje, M.C. Gallardo, J. Jiménez, F.J. Romero, and J. del Cerro, J. Phys.: Condens. Matter **10**, 5535 (1998).
[4] K.A. Müller, W. Berlinger, E. Tosatti, Z. Phys. B: Condens. Matter **84**, 277 (1991).
[5] E. Courtens, Ferroelectrics **183**, 25 (1996).
[6] B. Hehlen, Z. Kallassy, and E. Courtens, Ferroelectrics **183**, 265 (1996).
[7] B. Hehlen, L. Arzel, A.K. Tagantsev, E. Courtens, Y. Inaba, A. Yamanaka, and K. Inoue, Phys. Rev. B **57**, R13 989 (1998).
[8] O.M. Nes, K.A. Müller, T. Suzuki, and F. Fossheim, Europhys. Lett. **19**, 397 (1992).
[9] W. Rehwald, Solid State Commun. **8**, 1483 (1970).
[10] J.F. Scott and H. Ledbetter, Z. Phys. B: Condens. Matter **104**, 635 (1997).

[11] J.O. Fossum, K. Fossheim, and H.J. Scheel, Solid State Commun. **51**, 839 (1984).
[12] E.V. Balashova, V.V. Lemanov, R. Kunze, G. Martin, and M. Weihnacht, Ferroelectrics **183**, 75 (1996).
[13] G. Sorge, E. Hegenbarth, and G. Schmidt, Phys. Status Solidi **37**, 599 (1970).
[14] W. Schranz, D. Havlik, and M. Fally, Mod. Phys. Lett. B **9**, 1817 (1995).
[15] M.A. Carpenter and E.K.H. Salje, Eur. J. Mineral. **10**, 693 (1998).
[16] J.C. Slonczewsky and H. Thomas, Phys. Rev. B **1**, 3599 (1970).
[17] M. Liu, T.R. Finlayson, and T.F. Smith, Phys. Rev. B **55**, 3480 (1997).
[18] A. Buckley, J.P. Rivera, and E.K.H. Salje, J. Appl. Phys. **86**, 1653 (1999).
[19] A.V. Kityk, V.P. Soprunyuk, A. Fuith, W. Schranz, and H. Warhanek, Phys. Rev. B **53**, 6337 (1996).
[20] P.G. de Gennes, *The Physics of Liquid Crystals* (Clarendon, Oxford, 1975), p. 347.
[21] V.S. Boyko, R.I. Garber, and A.M. Kossevich, *Reversible Crystal Plasticity* (AIP, New York, 1994).
[22] E. Courtens, G. Coddens, B. Hennion, B. Hehlen, J. Pelous, and R. Vacher, Phys. Scr. **T49**, 430 (1993).
[23] J.M. Worlock, J.F. Scott, and P.A. Fleury, in *Light Scattering in Solids*, edited by G.B. Wright (Springer, New York, 1969), p. 689.
[24] D.W. Wilson and L.A. Carlson, in *Physical Methods of Chemistry*, edited by B.W. Rossister and R. C. Baetzold (Wiley, New York, 1991), Vol. VII, p. 178.
[25] Cheng Ang, J.F. Scott, Zhi Yu, H. Ledbetter, and J.L. Baptista, Phys. Rev. B **59**, 6661 (1999).